Land Subsidence Monitoring in Azar Oil Field Based on Time Series Analysis

Zahra Mirzaii [1], Mahdi Hasanlou [2],* Sami Samieie-Esfahany [3], Mahdi Rojhani [4], and Parviz Ajourlou [5]

School of Surveying and Geospatial Engineering, College of Engineering, University of Tehran; z_mirzaei@ut.ac.ir

[2] School of Surveying and Geospatial Engineering, College of Engineering, University of Tehran; hasanlou@ut.ac.ir

[3] School of Surveying and Geospatial Engineering, College of Engineering, University of Tehran ; s.samieiesfahany@ut.ac.ir

[4] Geotechnical Engineering, Shahed University ; m.rojhani@shahed.ac.ir

[5] School of Surveying and Geospatial Engineering, College of Engineering, University of Tehran ; Parviz.ajourlou@ut.ac.ir

* Correspondence: hasanlou@ut.ac.ir; Tel.: +98-21-6111-4525

Abstract: Azar Oil Field is located in the east of the city of Mehran, Ilam. The tank of this oil field is shared by Iraq's oil field whose name is Badra where oil extraction started in 2014, and they have maximized its oil exploration since 2017. Iran started oil exploration in 2017. In this study, we have estimated land surface deformation in Azar Oil Field using persistant scattering interferometry (PSI) to explore what the corresponding subsidence source is. PSI is a method of time series analysis to measure various surface deformations. The Stanford Method for Persistent Scatterers (StaMPS) package has been employed to process 50 ascending Sentinel-1A satellite images collected between 2016 and 2019, and 50 descending Sentinel-1A satellite images were collected between 2014 and 2019 to extract horizontal and vertical displacement components from the InSAR LOS (Line of Sight) displacement. The results show the maximum displacement rate in Iran-Iraq joint oil field was 15 mm between 2016 and 2019 in the vertical direction. Moreover, the maximum displacement rate measured in the horizontal direction was 30 mm. The vertical deformation confirms typical patterns of subsidence caused by oil extraction, and the horizontal deformation occurred due to considerable precipitations after a drought period, as well as the presence of sand layers at different depths of the earth.

Keywords: Azar oil field, Time series analysis, Persistent Scatterers, Land subsidence

1. Introduction

Land surface deformation has occurred in the Azar oil field. Between 2007 and 2011, the region observed sharp decreases in precipitation, but dramatic increases in the period between 2011 and 2013. The region's soil, regarded to be of a weak type, is categorized as sandstone in the international categorization. Since 2013, some cracks have formed which despite modifications still persist. Figure 1 shows some typical cracks in this region.

٣٨

٣٩ Figure 1. Sample of cracks observed in Azar Oil Field

٤٠ In order to monitor the region, once the cracks formed, a noticeable number of studies of different
٤١ types such as geotechnical, hydrological, meteorological, seismic, and geophysical were conducted.
٤٢ Drilling from Iraq's petroleum tank began in 2014, and Iran started to drill in 2017. The oil in this
٤٣ reservoir is worth around four billion, and it is planned to drill the whole amount within a 20-year
٤٤ period. The length of this tank is 36 km in the northeast, southwest direction, 13.5 km of which is
٤٥ located in Iran, and it extends along a width of 30 km. In Figure 2, we show Azar Oil Field,
٤٦ alongside 15 wells. Figure 3, in turn, displays the cracks formed in the region.

٤٧
٤٨   **(a)**   **(b)**

٤٩ **Figure 2.** (**a**) White polygon is Azar Oil Field and the blue line shows access roads to Azar Oil Field;
٥٠ (**b**) Sites and wells in this area
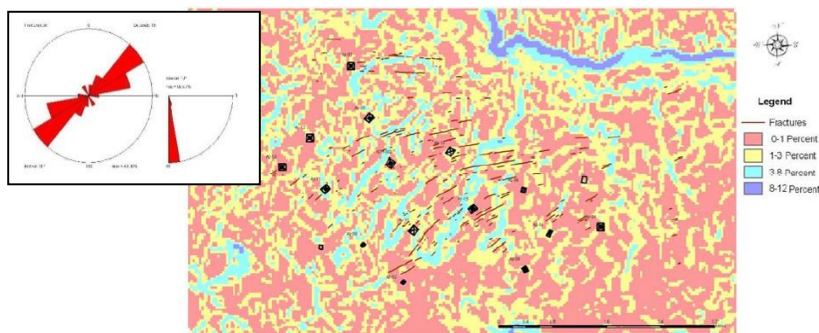
٥١
٥٢ **Figure 3.** Slope plan of the oil field and the distribution and direction of cracks in this area

٥٣ Azimuth direction of the cracks is between N45E to N85E, and most of the azimuth direction of
٥٤ cracks is N60-65E and N75-85E. Our goal in this article is to derive the temporal pattern of land
٥٥ deformation in this region using additional SAR data. C-band data from Copernicus missions

2

Sentinel-1A have some attractive properties such as large volumes of archived imagery, larger coverage/swath, and importantly, from the application point of view, free and open access data policy. We employ 50 descending Sentinel-1A satellite images were collected between 2014 and 2019, as well as 50 ascending Sentinel-1A satellite images were collected between 2016 and 2019.

Satellite Radar Interferometry (InSAR) method provides an all-weather, day-or-night capability to map ground deformations from human activities or various natural causes such as volcano dynamics, earthquakes, slope instability, groundwater overexploitation, mining, and coastland reclamation[1-7]. Any factor that can affect the phase of the backscattered radar signal can affect the deformation pattern. These measurements include surface displacements, land changes, land subsidence/uplift, water levels, soil moisture, snow accumulation, the volume of the forest, etc. Therefore, InSAR has found very broad applications in the field of earth and environmental sciences [8].

Land surface deformation leads to widespread damage to oil and drilling rigs, roads, and infrastructures. Knowledge of the spatial and temporal extent of land settlement provides important information to establish effective measures necessary to mitigate losses from the land subsidence hazard [9].

2. Experiments

The radar transmits a pulse to the earth and measures the return of the back-scattered pulses. The received pulses are digitized and make a raw complex data or a real aperture radar (RAR) image, with a very bad resolution in the flight direction because of physical length limitations of the radar antenna [10]. RAR images are subsequently focused by signal processing techniques so as to artificially make a long antenna and create a synthetic aperture radar (SAR) image with a much higher resolution. SAR images are sampled in an azimuth and range coordinate system, so every pixel has a unique range and azimuth coordinate. Single-look complex (SLC) data is a standard format of focused SAR images. the phase of SLC data can be written as a summation of four components as[10]:

$$\psi = W\{\psi^{range} + \psi^{atmo} + \psi^{scat} + \psi^{noise}\} \qquad (1)$$

where W{.} is the modulo-2π wrapping operator, ψ^{range} is related to the distance between the radar sensor, ψ^{atmo} the phase delay induced by the atmosphere ψ^{scat} is related to the distribution of all scatterers within a resolution cell, and ψ^{noise} the additional system or thermal noise which is dependent on sensor specifications[1]. the phase difference between two SAR images that are acquired from different positions or at different times is called interferograms. The interferogram is produced by complex conjugate multiplication of the two coregistered SLC images(P_{Master} and P_{Slave}). The interferometric phase ϕ_{MS} for a single pixel can be written as the summation of four components:

$$\phi_{MS} = W\{\psi_M - \psi_S\} = W\{\phi^{range} + \phi^{atmo} + \phi^{scat} + \phi^{noise}\} \qquad (2)$$

where ψ is the phase of SLC data and φ is the differential phase between two SLC data. The phase component range, atmosphere scatter, and noise can be further decomposed into some components that are shown in Figure 4:

3

Figure 4. Decomposition of interferometric phase [10]

٩٧   Our methods in this article are Persistent Scatter interferometry (PSI), so we have used Single Master
٩٨ (SM) interferometry. We have coregistered master and slave images together in three steps. Then we
٩٩ have produced 49 interferograms from 50 descending SLC images and 49 interferograms from 50
١٠٠ ascending SLC images. Flat earth and topographic phase are subtracted from every interferogram.
١٠١ We have carried out time series analysis in three main steps. We have used the phase stability with
١٠٢ respect to predefined model in space to select PS-pixels. Pixel candidates have been selected if their
١٠٣ interferometric phases have had a small deviation from their neighboring PS. After the selection of
١٠٤ PS, 3D unwrapping has been performed, and mitigation of atmospheric signal with high-pass
١٠٥ filtering in time and low-pass filtering in space has been conducted.

١٠٦ The dataset includes 50 ascending images between June 2016 and February 2019, 50 descending
١٠٧ images covering October 2014-February 2019 that are shown in Figure 5.

١٠٨

١٠٩
١١٠ **Figure5.** Topography map of Mehran, Ilam. The boxes show satellite trajectories of radar images for
١١١ descending orbits. The Blue box is Azar Oil Field.

١١٢

١١٣ We have produced interferograms with a single master. Interferometric combinations of the images were
١١٤ carried out with the consideration of their spatial and temporal baselines. The overview of the baseline
١١٥ perpendicular plot of the images can be seen in Figure 6.

Figure 6. Plots of acquisition dates versus perpendicular baselines for the final network of the (a) S1 descending, (b) S1 ascending, data are used for the time series analysis. The circles represent SAR images, and the lines represent interferograms.

To make sure there is no unwrapping error, we have generated ascending data interferograms with three masters. The results obtained from all these masters were almost the same, so there was no unwrapping error. The difference between deformation signals shown in ascending and descending processing is because of deformations in a horizontal direction.

3. Results

Deformation velocity maps in Iran-Iraq Joint oilfield and Azar oil field is shown in Figure 7.
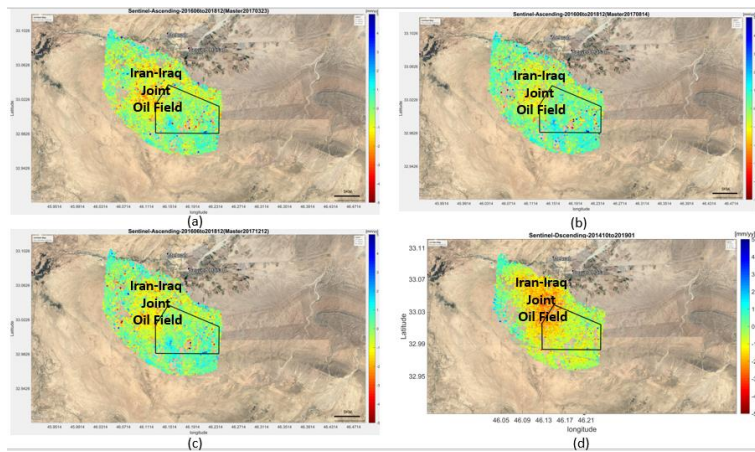
Figure 7. Deformation velocity map with the reference point (46.22, 33.02) (a) S1 ascending with master 20170323 (b) S1 ascending with master 20170814 (c) S1 ascending with master 20171212 (d) S1 descending with master 2017011. This polygon is Azar Oil Field.

As can be seen in Figure 7, displacement is observed in the ascending data velocity map between 2016 and 2019, and in descending data between 2014 and 2019. Owing to droughts during some years and subsequent precipitations, as well as the region's soil type and oil drilling, a 5-mm displacement per year, can be seen. The cumulative displacement diagram (Figure 8) for this period is presented below.

5

(a)   (b)
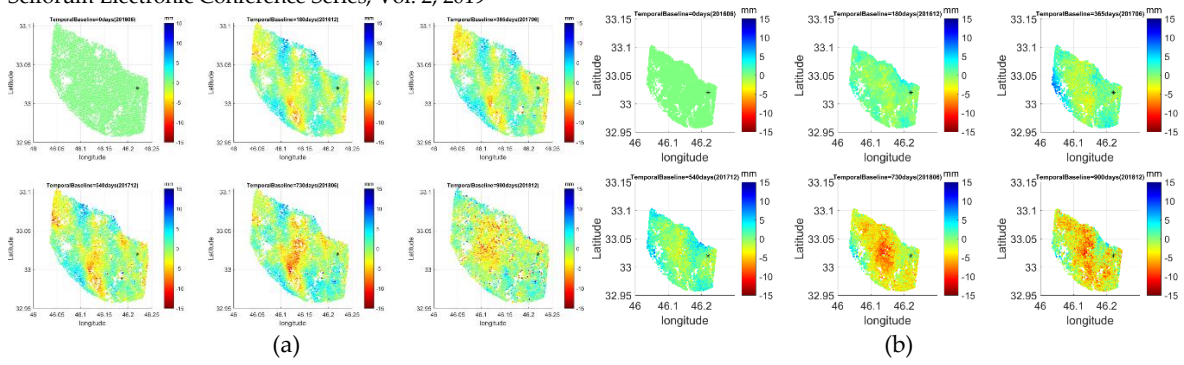
Figure 8. Cumulative displacement of Azar Oil Field obtained from 201606 to 201812 every six months (a) ascending Sentinel-1 (b) descending Sentinel-1

We used multi-track deformation estimate and we have utilized it to decompose deformation along line-of-sight into vertical and horizontal movements. We need to create a new grid to interpolate ascending and descending data on it to spatial coregister data. In Figure 9, We have shown the displacement between 201606 and 201812 with the reference point (46.22, 33.02) in the same grid:

(a)   (b)
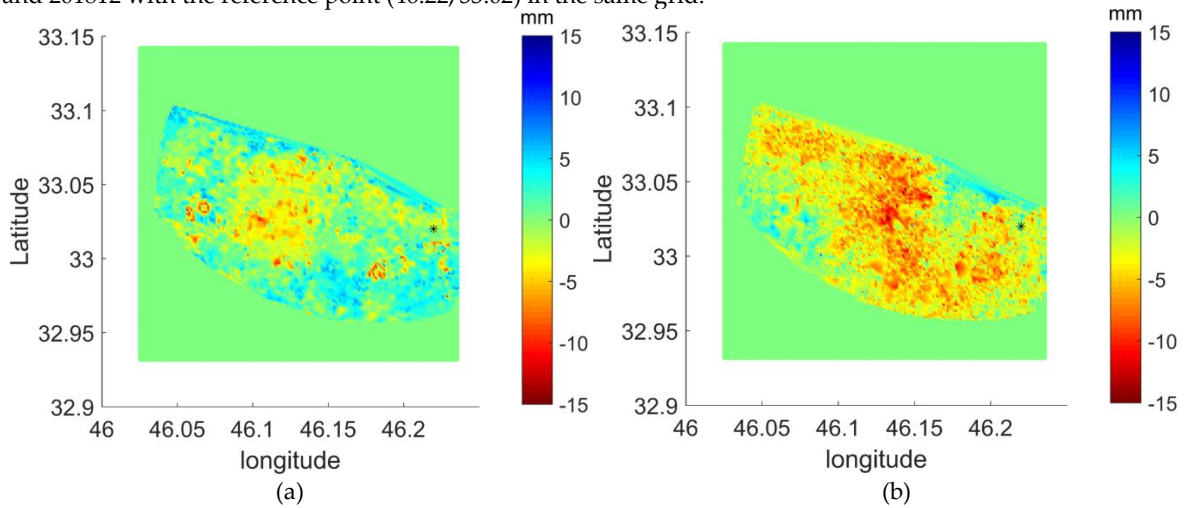
Figure 9. The displacement between 201606 and 201812 (a) ascending griding data (b) descending griding data with the reference point (46.22, 33.02) is shown in black

4. Discussion

Where in Figure 9, ascending and descending are the same there has been a vertical displacement which is located over Iran and Iraq's tank. Where there has been different in the line of sight direction, displacement has been horizontal. Figure 10 shows vertical displacement after decomposition.

6

١٥٨
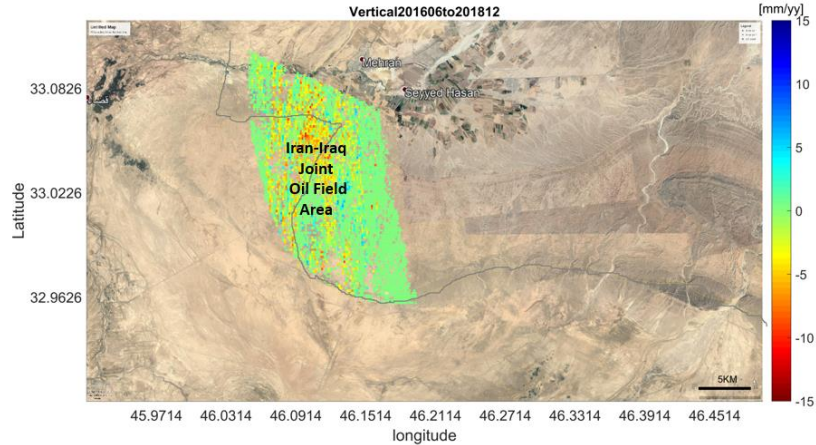
١٥٩ **Figure10.** Vertical displacement in Iran-Iraq Joint Oil Field area between 201606to 201812

١٦٠

١٦١ Figure 11 indicates horizontal displacement in Azar Oil Field which corresponds to the region's existing cracks.

١٦٢ This displacement has been caused by the existence of sand layers in depths of 10 to 15 meters under the

١٦٣ ground, which we discovered in geological studies. Droughts and subsequent considerable precipitations have

١٦٤ caused the soil on the sand layer to slide and inconsistent slides have resulted in different displacements in the

١٦٥ western direction and the formation of cracks.

١٦٦ In Figure 11 (a) Azar Oil Field and 15 wells that were excavated and the cracks formed in the region. These have

١٦٧ been obtained through various studies.

١٦٨

١٦٩ (a) (b)
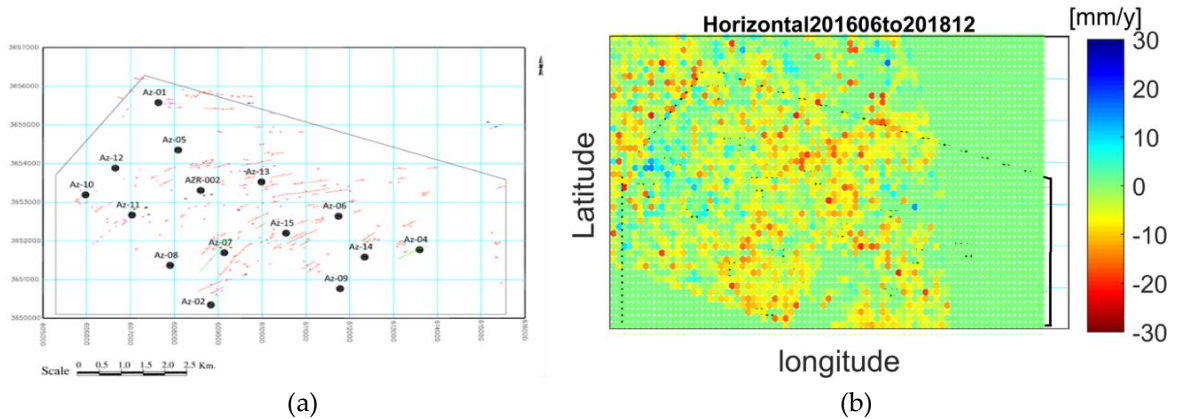
١٧٠ **Figure 11.** (a) Distribution of wells and cracks in Azar Oil Field (b) Horizontal displacement in Azar Oil Field area

١٧١ between 201606 and 201812

١٧٢

١٧٣ **5. Conclusions**

١٧٤ This study presents an application of the InSAR time series analysis to derive the spatial-temporal evolution of

١٧٥ land subsidence in Azar Oil Field. The PSI method was applied for a dataset of 98 interferograms in order to

١٧٦ extract surface deformation. The analyses also show that oil extraction plays a key role in land subsidence in

١٧٧ Azar Oil Field. Due to the high depth of oil wells (4,300 kilometers), we expect the subsidence to cover a large

١٧٨ area with a small magnitude. The subsidence is mainly observed in the vicinity of the oil field caused by fluid

١٧٩ extraction. Likewise, the result of the InSAR cumulative map may show seasonal displacements on the territory.

7

۱۸۰ Different horizontal displacement has been caused in the western direction. This has happened due to the inconsistent

۱۸۱ sliding of sand layers in depths of 10 to 15 meters, as well as considerable precipitations in the region.

۱۸۲ **References**

۱۸۳

۱۸۴ *1.* Massonnet, D.; Feigl, K. *Radar interferometry and its application to changes in the Earth's surface.*
۱۸۵ Rev. Geophys. 1998, 36, 441–500.

۱۸۶ 2. Q. Luo, D. Perissin, H. Lin, Y. Zhang and W. Wang. Subsidence Monitoring of Tianjin Suburbs by
۱۸۷ TerraSAR-X Persistent Scatterers Interferometry, IEEE Journal of Selected Topics in Applied Earth
۱۸۸ Observations and Remote Sensing, 2014, vol. 7, no. 5, pp. 1642-1650.

۱۸۹ 3. J. Yen, K. Chen, C. Chang and W. Boerner. Evaluation of earthquake potential and surface deformation by
۱۹۰ Differential Interferometry, Remote Sensing of Environment, 2008, vol. 112, no. 3, pp. 782-795.

۱۹۱ 4. L. Jiang, H. Lin, J. Ma, B. Kong and Y. Wang. Potential of small-baseline SAR interferometry for
۱۹۲ monitoring land subsidence related to underground coal fires: Wuda (Northern China) case study,
۱۹۳ Remote Sensing of Environment, 2011, vol. 115, no. 2, pp. 257-268.

۱۹۴ 5. B. Yu, G. Liu, Z. Li, R. Zhang, H. Jia, X. Wang and G. Cai. Subsidence detection by TerraSAR-X
۱۹۵ interferometry on a network of natural persistent scatterers and artificial corner reflectors, Computers &
۱۹۶ Geosciences, 2013, vol. 58, pp. 126-136.

۱۹۷ 6. H. Jung, S. Kim, H. Jung, K. Min and J. Won. Satellite observation of coal mining subsidence by persistent
۱۹۸ scatterer analysis, Engineering Geology, 2007, vol. 92, no. 1-2, pp. 1-13.

۱۹۹ 7. L. Jiang and H. Lin. Integrated analysis of SAR interferometric and geological data for investigating
۲۰۰ long-term reclamation settlement of Chek Lap Kok Airport, Hong Kong, Engineering Geology, 2010, vol.
۲۰۱ 110, no. 3-4, pp. 77-92.

۲۰۲ 8. X. Zhou, N. Chang and S. Li. Applications of SAR Interferometry in Earth and Environmental Science
۲۰۳ Research, Sensors, 2009, vol. 9, no. 3, pp. 1876-1912.

۲۰۴ 9. M. Motagh, et al. "Land subsidence in Iran caused by widespread water reservoir overexploitation," J.
۲۰۵ Geophys. Res letters, 2008, vol. 35, L16403, doi:10.1029/2008GL033814.

۲۰۶ 10. Sami Samiei Esfahany. *Exploitation of Distributed Scatterers in Synthetic Aperture Radar Interferometry*. PhD
۲۰۷ thesis, Delft University of Technology, 2017, Delft, the Netherlands.

۲۰۸